Energy & Environmental Science

ROYAL SOCIETY OF CHEMISTRY

PAPER

View Article Online
View Journal | View Issue

Cite this: *Energy Environ. Sci.*, 2025, **18**, 2395

Electrolytic cement clinker precursor production sustained through orthogonalization of ion vectors†

Zishuai Zhang, [a] Aubry S. R. Williams, [a] Shaoxuan Ren, [a] Benjamin A. W. Mowbray, [a] Colin T. E. Parkyn, [a] Yongwook Kim, [a] Tengxiao Ji [a] and Curtis P. Berlinguette *[abcd]

Received 21st October 2024,
Accepted 9th January 2025

DOI: 10.1039/d4ee04881d

rsc.li/ees

Electrochemical reactors can reduce the carbon intensity of cement production by using electricity to convert limestone ($CaCO_3$) into $Ca(OH)_2$, which can be converted into cement clinker by reacting with silica (SiO_2) at high temperatures. A key challenge with electrochemical reactors is that the deposition of solid $Ca(OH)_2$ at the membrane leads to unacceptably low energy efficiencies. To address this challenge, we connected the electrochemical reactor used for limestone calcination (''cement electrolyser'') to a distinctive chemical reactor (''calcium reactor'') so that $Ca(OH)_2$ forms in the calcium reactor instead of within the electrochemical reactor. In this tandem system, the cement electrolyser generates H^+ and OH^- in the respective chemical and cathode compartments. The H^+ then reacts with $CaCO_3$ to release Ca^{2+}, which is diverted into the calcium reactor to react with the OH^- to form $Ca(OH)_2$. We fabricated a composite membrane to selectively block the transport of Ca^{2+} into the cathode compartment. Charge balance in the cement electrolyser was enabled with monovalent ions (*e.g.*, K^+) as the positive charge carrier. This orthogonalized ion management was validated by *operando* imaging. The tandem reactor enabled the electrolysis process to operate for 50 hours at 100 mA cm^{-2} without any voltage increase, which represents a meaningful step forward for electrochemical cement clinker precursor production.

Broader context

Cement production is a significant source of global carbon emissions, partly because of the energy intensity of thermally converting limestone ($CaCO_3$) into cement clinker. To reduce this energy intensity, electricity can be used to convert limestone into calcium hydroxide ($Ca(OH)_2$), which can then be processed into cement clinker. A significant challenge in using an electrolyser to decompose limestone is the deposition of $Ca(OH)_2$ on the membrane that separates the reaction compartments. This deposition of $Ca(OH)_2$ reduces the energy efficiency of the system. To address this issue, we developed a tandem unit that connects an electrochemical reactor (''cement electrolyser'') with a chemical reactor (''calcium reactor''). In this tandem unit, the cement electrolyser produces hydrogen ions (H^+) and hydroxide ions (OH^-) in separate compartments. The H^+ ions react with $CaCO_3$ to form calcium ions (Ca^{2+}), which are diverted to the calcium reactor to form $Ca(OH)_2$ with the OH^- ions. A composite membrane that selectively blocks Ca^{2+} from entering the cathode compartment enabled the operation of this tandem reactor for 50 hours at 100 mA cm^{-2} without a voltage increase. This development represents a step forward in reducing the carbon footprint of cement production using electrochemical methods.

Introduction

Cement production accounts for ~8% of global CO_2 emissions,[1] primarily due to the production of cement clinker, the active component of cement.[2] The commercial production of cement clinker involves the thermal decomposition of limestone ($CaCO_3$) into CaO and CO_2 (~900 °C, eqn (1)). Heat generated from the combustion of fossil fuels drives this decomposition and releases significant amounts of CO_2 into the atmosphere.[1] Demonstrations of electrochemical reactors (''cement electrolysers'') have emerged that can convert $CaCO_3$

[a] *Department of Chemistry, The University of British Columbia, 2036 Main Mall, Vancouver, British Columbia, V6T 1Z1, Canada. E-mail: cberling@chem.ubc.ca*
[b] *Department of Chemical and Biological Engineering, The University of British Columbia, 2360 East Mall, Vancouver, British Columbia, V6T 1Z3, Canada*
[c] *Stewart Blusson Quantum Matter Institute, The University of British Columbia, 2355 East Mall, Vancouver, British Columbia, V6T 1Z4, Canada*
[d] *Canadian Institute for Advanced Research (CIFAR), 661 University Avenue, Toronto, M5G 1M1, Ontario, Canada*

† Electronic supplementary information (ESI) available. See DOI: https://doi.org/10.1039/d4ee04881d

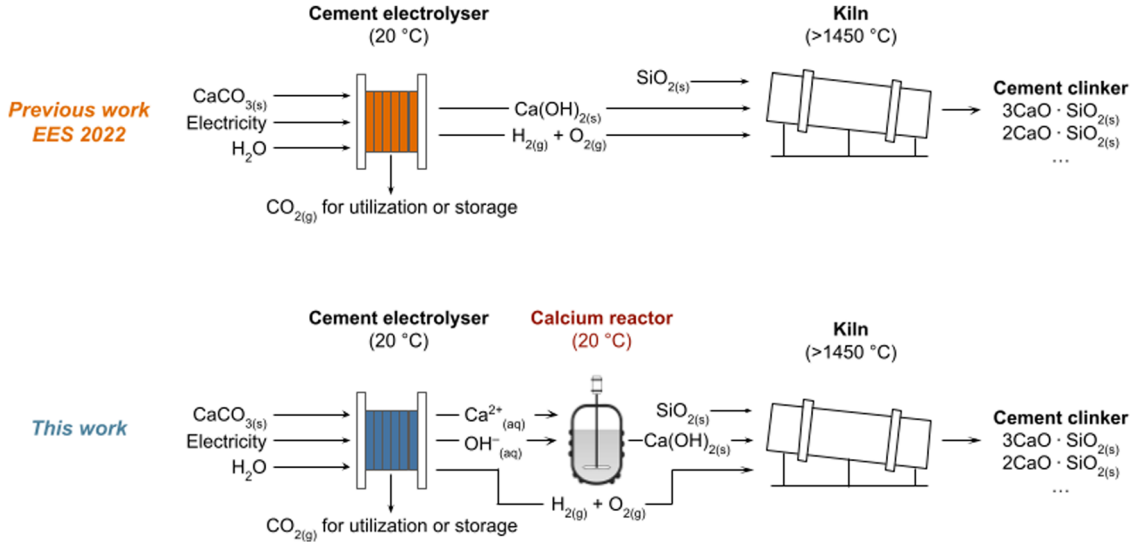

Fig. 1 Comparison of our previous electrochemical cement production scheme (top) and the proposed cement production scheme (bottom). In our previous work, $Ca(OH)_2$ was produced directly from a cement electrolyser as a precursor to cement clinker. In this new proposed scheme, Ca^{2+} and OH^- are produced from a cement electrolyser and then $Ca(OH)_2$ is produced in a calcium reactor. For both pathways, $Ca(OH)_2$ are converted into clinker by reacting with SiO_2 in a high-temperature kiln.

into $Ca(OH)_2$ (slaked lime; a cement clinker precursor) using renewable electricity to reduce CO_2 emissions from cement production.[1–4] The $Ca(OH)_2$ can then be reacted with SiO_2 to form cement clinker (>1450 °C, eqn (2)).[1] While these cement electrolysers eliminate only one of two high-temperature steps ($CaCO_3$ calcination, eqn (1)), they produce a pure stream of CO_2 byproduct that can be stored or converted into value-added products.[5–7] This electrochemical approach could reduce the carbon intensity of cement production by up to 75% (Fig. 1).[1]

$$CaCO_{3(s)} \rightleftharpoons CaO_{(s)} + CO_{2(g)} \quad (1)$$

$$3Ca(OH)_{2(s)} + SiO_{2(s)} \rightarrow 3CaO{\cdot}SiO_{2(s)} + 3H_2O_{(l)} \quad (2)$$

There are two key factors to consider when designing a cement electrolyser to decompose $CaCO_3$. The first is that $CaCO_3$ is not electrochemically active; it cannot be decomposed by electron transfer reactions at an electrode. However, $CaCO_3$ reacts with acid to form soluble Ca^{2+} and gaseous CO_2 (eqn (3)). A cement electrolyser must therefore continuously generate acid to drive the decomposition of $CaCO_3$ and generate the reactive Ca^{2+} needed to form the $Ca(OH)_2$ product. The second factor is that the two-step conversion of $CaCO_3$ into $Ca(OH)_2$ needs to occur at high production rates (*e.g.*, current densities, j, above 100 mA cm^{-2}). Consequently, a cement electrolyser must effectively manage the collective transport of the $CaCO_3$ feedstock, reactive Ca^{2+}, and $Ca(OH)_2$ product.

We addressed these points by designing an electrolyser that consisted of three compartments: an anode compartment for oxygen generation; a cathode compartment for hydroxide generation; and a chemical compartment situated between the anode and cathode compartments for $CaCO_3$ decomposition with acid (Fig. 2).[1] A bipolar membrane (BPM) separated the anode and chemical compartments, and a cation exchange membrane (CEM) separated the chemical and cathode compartments. The BPM delivered H^+ into the chemical compartment to react with $CaCO_3$ (eqn (3)).[8–14] In the anode compartment, the oxygen evolution reaction (OER) consumed the generated OH^-. In the cathode compartment, the hydrogen evolution reaction (HER) generated H_2 and OH^- to create an alkaline environment with a pH of $\sim$12 (eqn (4)).[1] The working principle of the cement electrolyser is that Ca^{2+} generated in the chemical compartment passes through the CEM and enters the cathode compartment to react with OH^- and form $Ca(OH)_2$ (eqn (5) and Fig. 2). At the anode, the OER generates a pure O_2 stream that can be combusted with the H_2 generated at the cathode as a source of heat for thermal steps in cement production (Fig. 1).[1]

$$CaCO_{3(s)} + 2H^+_{(aq)} \rightleftharpoons Ca^{2+}_{(aq)} + CO_{2(g)} + H_2O \quad (3)$$

$$2H_2O \rightarrow 2OH^-_{(aq)} + H_{2(g)} + 2e^- \quad (4)$$

$$Ca^{2+}_{(aq)} + 2OH^-_{(aq)} \rightarrow Ca(OH)_{2(s)} \quad (5)$$

This cement electrolyser was capable of operating at a current density of 100 mA cm^{-2} with 100% current efficiency and enabled the highest rates of electrochemical $Ca(OH)_2$ formation reported in the literature to date (486 mg h^{-1}). However, this electrolyser was not able to sustain operation for extended time periods without incurring a massive increase in cell voltage (Fig. S1, ESI†). This drop in electrolyser performance occurred due to $Ca(OH)_2$ deposition at the CEM (Nafion™), which stunted Ca^{2+} transport into the cathode compartment (Fig. S2, ESI†). This factor, as well as a decrease in membrane conductivity caused by strong Ca^{2+} binding and consequent membrane dehydration,[15] led to a significant increase in cell voltage within hours (Fig. S1 and S2, ESI†). A robust cement electrolyser capable of sustained continuous

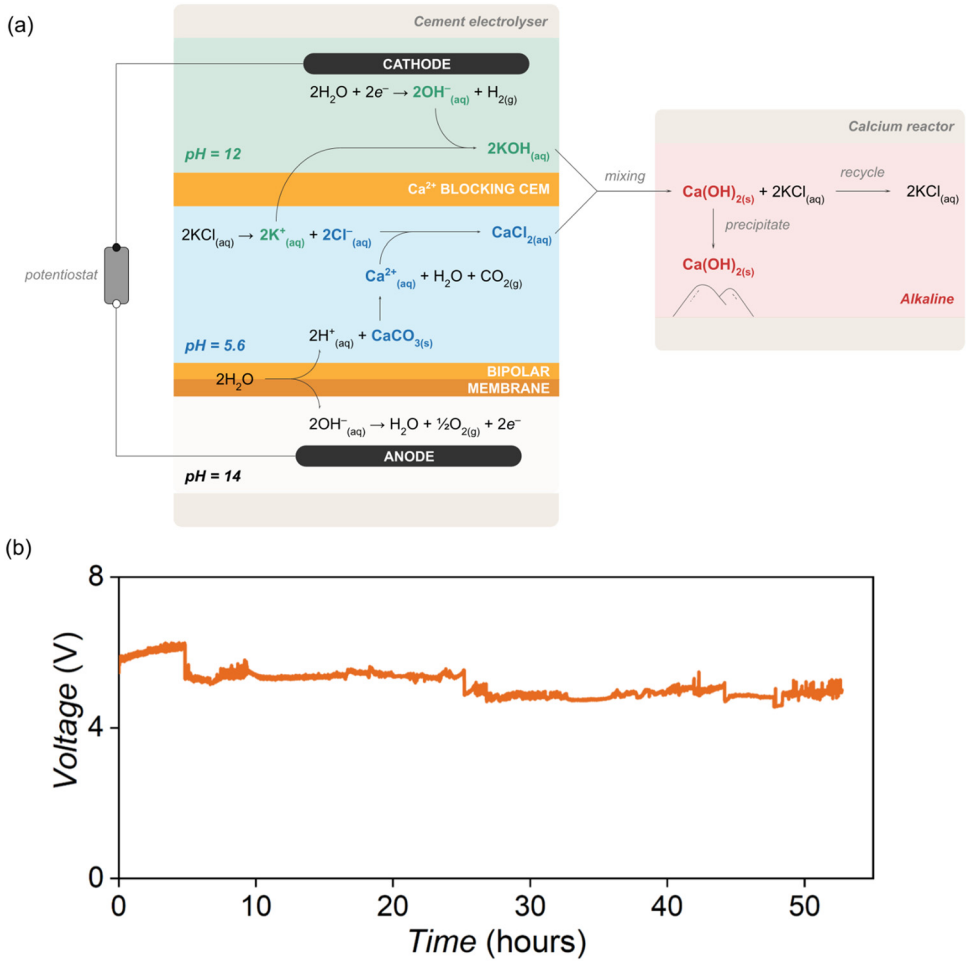

Fig. 2 Orthogonalization of ion vectors enables sustained electrolytic synthesis of cement clinker precursor. (a), Schematic representation of the dominant chemical and electrochemical reactions occurring in the cement electrolyser that contains a Ca^{2+}-blocking cation exchange membrane (CEM). A bipolar membrane (BPM) and a Ca^{2+}-blocking CEM separate the anode and chemical compartments, and the chemical and cathode compartments, respectively. The BPM generates H^+ for the reaction with $CaCO_3$ which releases Ca^{2+}. In the cathode compartment, HER produces H_2 and OH^-. Ca^{2+} and OH^- are directed to a calcium reactor outside the cell to produce $Ca(OH)_2$. K^+ serves as the charge carrier across the Ca^{2+}-blocking CEM. (b), The long-term durability of a cement electrolyser that contains a Ca^{2+}-blocking membrane and operates at 100 mA cm^{-2}. The voltage of the cement electrolyser with a Ca^{2+}-blocking membrane remains stable at around 5 V for 50 hours. We used a "simulated scenario" where the $[Ca^{2+}]$ is at 0.05 M and the $[K^+]$ is at 1 M. The electrolyte was refreshed every 6–8 hours. A trace amount of Ca^{2+} was detected in the catholyte during the entire electrolysis. Excessive $CaCO_3$ was added into the chemical compartment to consume H^+ from BPM.

operation (*i.e.*, >100 hours) would manage the transport of Ca^{2+} more effectively to avoid $Ca(OH)_2$ deposition on the membrane.

We report here a cement electrolyser that can sustain operation at 100 mA cm^{-2} for at least 50 hours. The electrolyser was designed to use potassium ions (K^+) rather than calcium ions (Ca^{2+}) as the positive charge carrier between the chemical and cathode compartments (Fig. 2). Unlike Ca^{2+}, K^+ does not form an insoluble deposit with OH^- on the CEM or dehydrate the CEM. Moreover, the ionic mobility of K^+ (~30 mS cm^{-1})[16] is higher than Ca^{2+} (~14 mS cm^{-1}),[17] which increases the energy efficiency of the cement electrolyser.[16,17] We designed a composite CEM to selectively block Ca^{2+} and accommodate the selective transport of K^+ (Fig. 2). When K^+ is forced as the main charge carrier across the membrane, Ca^{2+} and OH^- accumulate in the chemical and cathode compartments, respectively, during electrolysis. We directed these ions out of the cement electrolyser and into a "calcium reactor" where $Ca(OH)_2$ was formed (Fig. 1 and 2). This cement electrolyser and calcium reactor in tandem orthogonalized the transport of ions to enable the continuous conversion of $CaCO_3$ into $Ca(OH)_2$ at a current density of 100 mA cm^{-2} and voltage of ~5 V over 50 hours. This report is the first demonstration of sustained cement clinker precursor production at high current densities.

Results

Design of electrochemical reactors for $Ca(OH)_2$ production

This study was conducted using both a previously reported cement electrolyser design[1] and a modified cement electrolyser with a calcium reactor. In the typical three-compartment

cement electrolyser (Fig. S2, ESI†), the anode and cathode compartments were supplied with 1 M potassium hydroxide (KOH) and 1 M potassium chloride (KCl) solutions, respectively, and the chemical compartment was supplied with an aqueous slurry of $CaCO_3$ microparticles in 1 M KCl at a flow rate of 300 mL min^{-1}. For the 50-hour experiments, additional $CaCO_3$ was added to the electrolyte reservoir after 24 h. A BPM (Fumasep FBM) separated the anode and chemical compartments, and a CEM (Nafion™ 117) separated the chemical and cathode compartments. The primary difference in the modified cement electrolyser was the use of a composite CEM in place of a pristine Nafion™ membrane. This composite membrane blocked Ca^{2+} transport and instead enabled K^+ to be selectively transported across the CEM, which caused Ca^{2+} and OH^- to accumulate in the chemical and cathode compartments, respectively. The Ca^{2+} and OH^- enriched electrolytes from the chemical and cathode compartments were then manually mixed in a calcium reactor (specifically a 200 mL beaker) to form the $Ca(OH)_2$ product (Fig. 2). The precipitated $Ca(OH)_2$ was filtered from the mixed electrolyte so that the remaining KCl solution could be treated and reused. This stepwise $CaCO_3$-to-$Ca(OH)_2$ conversion process demonstrates the feasibility of the hybrid electrochemical and chemical method for $Ca(OH)_2$ production, and future work could involve building a fully automated system.

Design and fabrication of a composite membrane to block Ca^{2+} transport

To establish a baseline for the durability of the cement electrolyser, we ran an electrolysis experiment using a pristine Nafion™ membrane (positioned between the chemical and cathode compartments) under constant current conditions. The cell voltage (V_{cell}) increased from 5 V to 8 V within 60 minutes of electrolysis at 100 mA cm^{-2} (Fig. S1, ESI†). After disassembling the cell, we observed white deposits on the cathode-facing side of the Nafion™ membrane. Scanning electron microscopy (SEM) and X-ray fluorescence (XRF) images indicated the deposits consisted of a calcium-containing species (Fig. S2, ESI†), and Fourier transform infrared spectroscopy (FTIR) confirmed the precipitates consisted primarily of $Ca(OH)_2$ with trace amounts of $CaCO_3$ (Fig. S3, ESI†). We also observed that the Nafion™ membrane became dehydrated and developed wrinkles and cracks. The pliable texture of the Nafion™ membrane also became rigid (Fig. S4, ESI†).

To circumvent the deleterious effects of $Ca(OH)_2$ deposition on the membrane, we set out to prevent Ca^{2+} from transporting through the CEM as the charge carrier. We fabricated a composite CEM that permitted only monovalent ion transport and blocked divalent ions such as Ca^{2+} (Fig. 3). We deposited layers of polyaniline (PANI) on both sides of a Nafion™ 117 membrane.[18] The PANI-modified membrane was prepared by ion exchange of the protons in a pristine Nafion™ membrane with protonated aniline. Potassium persulfate ($K_2S_2O_8$) was then used to polymerize aniline into PANI. The composite membrane was then stored in a hydrochloric acid (HCl) solution for 24 hours to ensure the PANI layer was fully protonated (*i.e.*, positively charged). Following these steps, the composite membrane turned a translucent dark green colour in contrast to the translucent colourless appearance of pristine Nafion™. Scanning electron microscopy (SEM) images indicated the

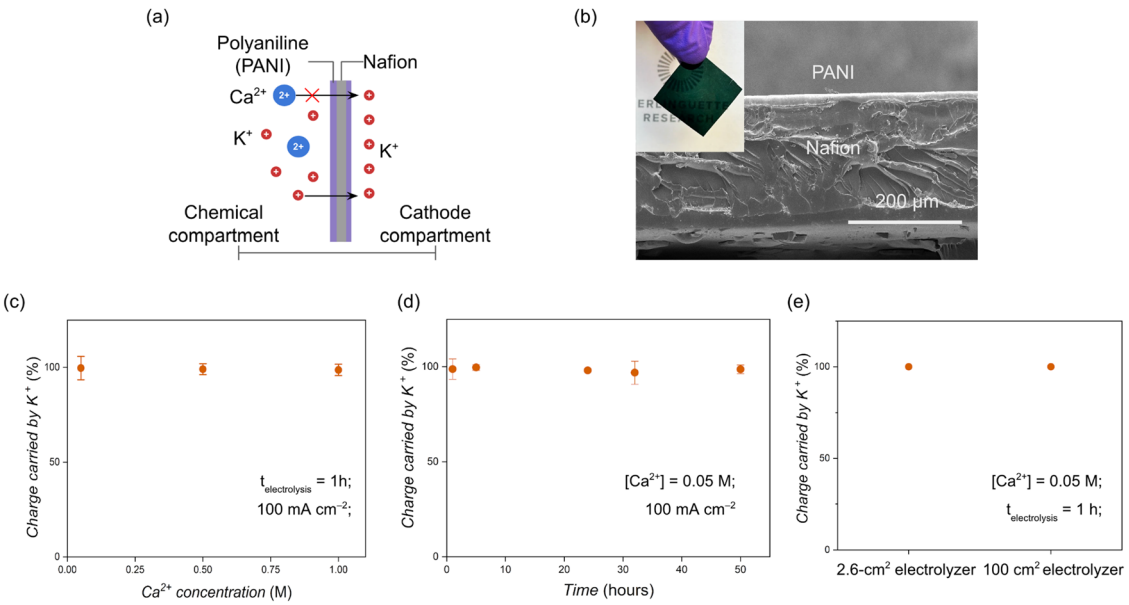

Fig. 3 Characterization of the composite membrane that blocks Ca^{2+}. (a) Illustration of the composite membrane that selectively blocks Ca^{2+}. (b) Photo and SEM image of a composite membrane that consists of a Nafion™ membrane with PANI layers. The insert figure is an optical photo of the composite membrane. Charge carried by K^+ through a composite membrane at various [Ca^{2+}] (c) and times (d) at 100 mA cm^{-2}. (e) K^+ carried 100% of charge in both 2.6 and 100 cm^2 electrolysers with 0.05 M $CaCl_2$ in 1 M KCl electrolyte after one hour of electrolysis. Excess $CaCO_3$ was added to the chemical compartment to exhaust H^+. The 100 cm^2 electrolyser was operated at 50 mA cm^{-2} with a total current of 5 A, and the 2.6 cm^2 electrolyser was operated at 100 mA cm^{-2}. All experiments were performed in triplicate, the error bars are within the size of the data point as plotted.

prepared PANI layers were roughly 5–10 μm thick and free of defects such as pinholes and large pores (Fig. 3).

Sustained electrochemical $Ca(OH)_2$ production enabled by a Ca^{2+}-blocking membrane

To evaluate the Ca^{2+}-blocking capacity of the composite membrane, we modulated the $CaCl_2$ concentration in the $CaCO_3$ slurry fed to the chemical compartment of the cement electrolyser and monitored the amount of Ca^{2+} passing through the membrane during electrolysis. Excess $CaCO_3$ was added to the slurry to consume H^+ generated by the BPM and ensure the charge carrier across the composite membrane was only K^+.[1] We measured the concentration of calcium ions ($[Ca^{2+}]$) in the cathode compartment over the course of each experiment using inductively coupled plasma optical emission spectrometry (ICP-OES) and used this data to calculate the charge carried by K^+ across the CEM (details are shown in the Methods section and Tables S1 and S2, ESI†). We found the composite membrane blocked ~100% of Ca^{2+} from crossing into the cathode compartment over a wide range of $[Ca^{2+}]$, specifically from 0.05 to 1.0 M (Fig. 3).

We also measured the charge carried by K^+ through the composite membrane over 50 hours of electrolysis. A constant $[Ca^{2+}]$ of 0.05 M was used to match the $[Ca^{2+}]$ measured in the chemical compartment after 120 minutes of electrolysis at 100 mA cm^{-2}. Periodic deposition of $Ca(OH)_2$ in the calcium reactor prevented the $[Ca^{2+}]$ from exceeding 0.05 M. We found the composite membrane demonstrated ~100% Ca^{2+} blockage over the 50 hour test period (Fig. 3). We verified the robustness of the PANI layer by performing FTIR (Fig. S5, ESI†) and SEM (Fig. S6, ESI†) on the composite membrane before and after the 50-hour test. We observed no change in the FTIR spectra, and the PANI layer appeared intact after the 50-hour test. (Fig. S7, ESI†). We also fabricated a much larger composite membrane for testing in a zero-gap electrolyser with an active area of 100 cm^2 to explore the scalability of the composite membrane. This experiment was again performed with a $[Ca^{2+}]$ of 0.05 M and a $[K^+]$ of 1 M in the 100 cm^2 electrolyser, which we operated at 50 mA cm^{-2}. The membrane maintained 100% charge carried by K^+ when operating at a total current of 5 A (Fig. 3 and Fig. S8, ESI†).

When the composite membrane was used in the modified cement electrolyser, concentrations of Ca^{2+} and OH^- in the chemical and cathode compartments, respectively, increased stoichiometrically during electrolysis. We manually mixed the Ca^{2+}-rich and OH^--rich electrolytes in the calcium reactor after two hours of electrolysis at 100 mA cm^{-2}. The Ca^{2+}-blocking membrane in the cement electrolyser coupled with the calcium reactor enabled the cement electrolyser to operate for 50 hours with a stable cell voltage (Fig. 2). A ''simulated scenario'' was used for the durability test wherein $[Ca^{2+}]$ was maintained at 0.05 M (the $[Ca^{2+}]$ in the electrolyte after 120 minutes of electrolysis at 100 mA cm^{-2}) and $[K^+]$ was set at 1 M. To maintain a constant $[Ca^{2+}]$, the electrolyte in the chemical compartment was refreshed every 6–8 hours and the catholyte was regularly monitored to confirm that no detectable Ca^{2+} had crossed the membrane. We observed a 0.4 V increase in cell voltage at 100 mA cm^{-2} compared with the pristine Nafion™ membrane, where the voltage increased by 2 V. This prolonged stability is a notable improvement on the previous electrolyser containing a pristine Nafion™ membrane. However, we initially observed $CaCO_3$ impurity in the $Ca(OH)_2$ product in the calcium reactor. We removed unreacted $CaCO_3$ from the chemical compartment electrolyte by centrifuging the mixture at 3000 rpm for 10 minutes before mixing. We hypothesized that the HCO_3^- in the chemical compartment reacts with the OH^- from the catholyte to form CO_3^{2-} which then reacts with Ca^{2+} to form $CaCO_3$. To mitigate this effect, we mixed the electrolytes in the calcium reactor only when the chemical compartment was below a pH of 5, which significantly decreased the $CaCO_3$ impurities in $Ca(OH)_2$.

We ran an additional experiment where we tested the pH in each compartment of the cement electrolyser containing the composite membrane every 30 minutes for two hours with a pH probe. We found that both the chemical and cathode compartments rapidly approached steady pH values of 5.6 and 13.5, respectively, with a significant pH change in both compartments within the first 30 minutes (Fig. S9, ESI†). The chemical compartment pH decreased from 9.9 to 6.1 in 30 minutes, and then to 5.6 by the end of the experiment (total experiment time of 2 hours). The cathode compartment became more basic with pH increasing from 8.8 to 12.9 in 30 minutes and then to 13.5 by the end of the 2-hour experiment. The anode compartment pH did not vary significantly from its starting value of 13.8.

Purity of the electrochemical $Ca(OH)_2$

The American Society for Testing and Materials (ASTM) sets limits on the allowable amounts of potassium and chlorine in cement clinker because of their potential to adversely affect the finished product.[19–21] In our study, we filtered out the solid $Ca(OH)_2$ product after mixing the Ca^{2+}-rich and OH^--rich electrolytes in the calcium reactor. The volume loss during filtration was consistently 2.5 ± 0.5 mL, independent of the total volume filtered, which ranged from 100–500 mL. This corresponds to KCl recovery efficiencies between 97.5–99.5%. After filtration, the solid product (~1.5 g) was rinsed with 3 × 50 mL of water and then dried in an oven at 60 °C for at least 24 hours before analysis. The $Ca(OH)_2$ particles had an average size of 1.45 ± 0.13 μm, as determined by SEM (Fig. S10, ESI†). This value closely matches the typical particle size of ~4 μm found in commercial $Ca(OH)_2$.[22]

ICP-OES was used to quantify the amount of potassium retained in the $Ca(OH)_2$ product from the supporting electrolyte. A dilution series of KCl in 2 wt% HNO_3 was prepared to generate a calibration curve for potassium concentrations. The amount of residual potassium in the isolated product was determined using a 40 000 ppm solution of the electrochemically produced $Ca(OH)_2$ prepared with 2 wt% HNO_3. The results indicated a potassium concentration of 62.5 ± 4.2 ppm, equating to 0.16 ± 0.011 wt% potassium in the solid $Ca(OH)_2$. This is less than the ASTM limit of alkali metals (K and Na) allowed in cement according of 0.60 wt%.[19] To supplement the ICP-OES

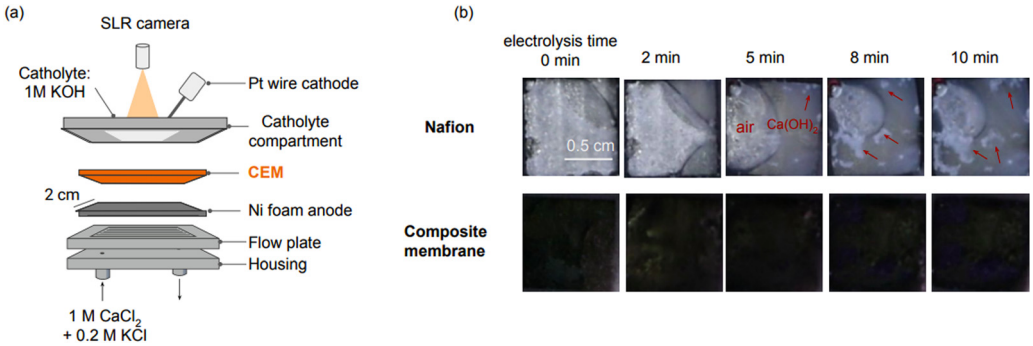

Fig. 4 Customized *operando* imaging system for $Ca(OH)_2$ deposit observation. (a) Schematic representation of the *operando* imaging system. 1 M $CaCl_2$ with 0.2 M KCl solutions were fed into the anode compartment and 1 M KOH was added to the catholyte reservoir. A Pt wire was placed in the catholyte reservoir as the cathode. The current density was maintained at 100 mA cm^{-2} during electrolysis. (b) Optical pictures of $Ca(OH)_2$ deposit nucleation and growth processes at different time scales (observation window is 1 × 1 cm). An air bubble was trapped between the anode and membrane due to the orientation of the electrolyser.

results, the $Ca(OH)_2$ product was also characterized by X-ray diffraction (XRD; Fig. S11, ESI†). No KCl or $CaCl_2$ was observed in the diffractogram, supporting the purity of the electrochemically produced $Ca(OH)_2$.

Conversion of $Ca(OH)_2$ into calcium silicates

The electrochemical $Ca(OH)_2$ was then converted into calcium silicates by thermal treatment with SiO_2. We mixed $Ca(OH)_2$ with SiO_2 particles in a mortar and pestle and then transferred the mixture to a Pt crucible. The crucible was placed in a kiln and heated to a temperature of 1050 °C and held for 2 hours to form dicalcium silicate ($2CaO{\cdot}SiO_2$; Fig. S12, ESI†), and 1500 °C to form tricalcium silicate ($3CaO{\cdot}SiO_2$; Fig. S12, ESI†).

Operando imaging system to diagnose membrane failure modes

We designed an *operando* imaging system to directly visualize $Ca(OH)_2$ deposition on the CEM and diagnose this membrane failure mode in real time (Fig. 4). The imaging system consisted of a modified two-compartment electrolyser with an open cathode compartment so we could image the CEM through the transparent catholyte with a high-resolution single-lens reflex (SLR) camera fixed above the electrolyser (Fig. 4 and Fig. S13, ESI†). A 1 M KOH solution was used as the catholyte to mimic the alkaline conditions of the chemical compartment in a cement electrolyser. A Pt wire was immersed into the catholyte to serve as the cathode. The anode on the opposite side of the CEM consisted of nickel (Ni) foam to facilitate the OER. Ni foam is an inexpensive, porous, and high surface area electrode material that is ideal for use as an OER electrocatalyst. The anode compartment was fed with an electrolyte containing 1 M $CaCl_2$ and 0.2 M KCl through a serpentine flow plate pressed directly against the Ni foam. This mixed electrolyte solution created a scenario where Ca^{2+} and K^+ could both serve as charge carriers across the CEM. We performed experiments using this setup with both pristine Nafion™ 117 and the PANI-modified composite membrane. With the pristine Nafion™ membrane, where Ca^{2+} was the charge carrier across the CEM, we observed the immediate formation of white $Ca(OH)_2$ precipitates on the CEM surface that faced the cathode. These $Ca(OH)_2$ precipitates (white spots in Fig. 4) formed on the Nafion™ membrane within five minutes of electrolysis at 100 mA cm^{-2} (Fig. 4) and grew in size over time. In contrast, no precipitate formed on the composite membrane. The high-resolution camera also detected the presence of bubbles trapped between the anode and CEM from the vertical orientation of the electrolyser, which was required to perform imaging.

Energy and CO_2 emission analysis

We calculated the energy required to convert $CaCO_3$ into cement when using our cement electrolyser and compared it to the conventional thermal process (Fig. 5). We also calculated the net CO_2 emissions per ton of cement for both methods (Fig. 6). The system boundary for the electrochemical pathway includes the electrolytic conversion of $CaCO_3$ to $Ca(OH)_2$, followed by its conversion to clinker in a kiln. In contrast, the system boundary for the thermal process includes the direct conversion of $CaCO_3$ to clinker in a kiln. We modeled both processes based on a hypothetical production capacity of 3000 tons of cement per day, assuming 95 wt% of the product is clinker, and the clinker is 65 wt% CaO.

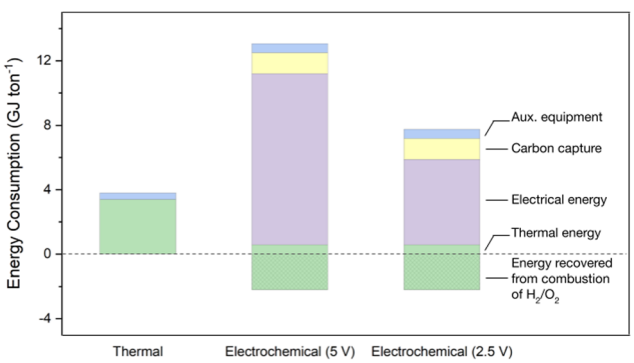

Fig. 5 Energy comparison for the production of 1 ton of cement *via* the conventional thermal pathway *vs.* electrochemical cement clinker precursor production at V_{cell} = 5 V (current performance) and 2.5 V (optimistic case).

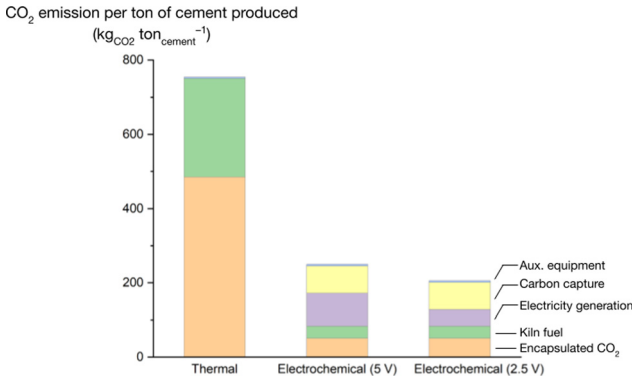

Fig. 6 Comparison of net CO_2 emissions for production of 1 ton of cement *via* conventional thermal pathway *vs.* electrochemical cement clinker precursor production at V_{cell} = 5 V (current performance) and 2.5 V (optimistic case) with carbon capture. To calculate the emissions from the electrochemical processes, we used a grid emissions intensity of 0.030 kg CO_2 kWh^{-1}, the same as that for the Province of Ontario,[23] where the majority of Canada's cement is produced.[24]

For the thermal process, 3.4 GJ of thermal energy is required per ton of cement,[25] provided by a fuel mix that would be used at a Canadian cement factory: 28% natural gas, 27% coal, 35% coke, 2% fuel oil, and 8% waste tires.[26] The emissions intensity of the kiln fuel was calculated to be 87.3 kg_{CO_2} GJ^{-1}.[27] Additional energy for auxiliary equipment (*e.g.*, pumps, conveyors, crushers) adds approximately 0.4 GJ, bringing the total to 3.8 GJ ton^{-1} of cement.

In the electrochemical pathway, we considered two scenarios: one using the cell voltage reported in this study (5 V, Fig. 2); and another optimistic scenario where the cell voltage has been reduced by half to 2.5 V, which has been demonstrated to be feasible in prior work.[28] In both cases, the electrical energy required to decompose limestone dominates the total energy input, with values of 10.6 GJ ton^{-1} and 5.3 GJ ton^{-1} of cement for the 5 V and 2.5 V cases, respectively. Both systems need an additional 2.8 GJ ton^{-1} of cement to convert $Ca(OH)_2$ into clinker.[2] However, the eletrochemical reactors also generate pure streams of H_2 and O_2, which can be combusted to supply most of the thermal energy of this step. If combusted with a thermal efficiency of 70%, the H_2 and O_2 streams supply 2.2 GJ ton^{-1} of cement. Retrofits will be required to safely handle and burn these gas streams due to the flame characteristics of H_2 and its potential to embrittle stainless steel.[29–31] Hydrogen blending has already been successfully demonstrated in several cement kilns.[32–34]

The electrochemical process also produces a stream of pure CO_2 from the chemical compartment of the electrolyser when $CaCO_3$ reacts with acid. Our model assumes 90% of this CO_2 is captured by an amine scrubber with a reboiler duty of 3 MJ kg^{-1} of CO_2.[35] The reboiler and balance of the secondary kiln are fueled by pure natural gas for the electrochemical processes. Carbon capture is not considered for the thermal process as it remains very rare at established cement plants.[35–38] The largest carbon capture unit currently operational at a cement plant, located at the Baimashan Cement Factory in Anhui, China,[39] captures 50 000 tons of CO_2 annually, much less than 1% of the company's annual CO_2 emissions of 183 million tons.[40]

The low adoption of carbon capture at cement factories is due to sorbent degradation from O_2, NO_x, and SO_x in flue gas,[41–43] difficulty in retrofitting existing cement plants with large carbon capture units,[44] and high capital and operating costs.[45] In prior work we demonstrated that the CO_2 emitted from the electrolyser chemical compartment can be fed directly into a CO_2 electrolyser for conversion into valuable products.[1]

Discussion

Our previously reported cement electrolyser electrochemically generated acid in a chemical compartment to decompose limestone into Ca^{2+}, which migrated across a CEM into a cathode compartment to react with OH^- and form $Ca(OH)_2$. The challenge with this setup was $Ca(OH)_2$ deposited on the surface of the CEM during electrolysis, which impeded additional Ca^{2+} transport into the cathode compartment. This deposition caused the cement electrolyser to exhibit voltages much higher than 5 V.

This study describes our effort to address the calcium deposition to achieve sustained cement electrolysis. To directly observe the $Ca(OH)_2$ deposition on the membrane surface, our *operando* imaging system featured an electrolyser with an open cathode compartment. This cathode compartment resembled a batch-type cathode compartment without a flowing catholyte to improve visualization and provide favourable conditions for precipitate formation.

We observed that $Ca(OH)_2$ deposited on the pristine Nafion™ membrane within five minutes of electrolysis. The spatial location of the deposits on the membrane appeared to have been influenced by the catholyte flow. Specifically, we observed that $Ca(OH)_2$ deposits initially formed near the compartment walls or as static bubbles when the catholyte flow was stagnant (Fig. 4). The initial deposits served as ''seeds'' for subsequent $Ca(OH)_2$ accumulation. These observations provide insight into how $Ca(OH)_2$ deposition occurs and can inform alternate mitigation strategies.

In our first experiment, we attempted to remove the $Ca(OH)_2$ deposits (when $\Delta V > 2$ V) by periodically treating the CEM with acid (*i.e.*, HCl). The acid treatment appeared to remove $Ca(OH)_2$ deposits from the membrane surface, but not the Ca^{2+} bound within the membrane. This experiment proved that V_{cell} could be recovered when the $Ca(OH)_2$ deposits were promptly removed (Fig. S14, ESI†), but would not recover after three hours of electrolysis. We attribute this irreversibility in voltage to the strong binding of Ca^{2+} to the sulfonic groups in Nafion™ membranes, which decreased H_2O diffusion and membrane conductivity.[15]

We then set out to use membranes that would prevent the transport of Ca^{2+} across the CEM. Selective blocking of divalent cations (*e.g.*, Ca^{2+}, Mg^{2+}) across CEMs has been reported in the fields of electrodialysis and water treatment, where chemical, mechanical, and electrochemical techniques have been used to

modify ion-exchange membranes.[46,47] Prior reports achieved this goal by applying a PANI coating to the surface of CEMs. This strategy increases K^+ permselectivity by leveraging increased electrostatic repulsion between the modified cationic surface of Nafion™ (*i.e.*, emeraldine-based PANI) and divalent cations in comparison to monovalent K^+. We borrowed from these fields to chemically modify the surface of Nafion™ with thin PANI layers to design a composite membrane for exceptional selectivity for monovalent cation transport (*i.e.*, K^+).[46] We observed high K^+ selectivity over Ca^{2+} when using this composite membrane. We attribute this result to three reasons. First, the larger size of hydrated Ca^{2+} (effective radii = 0.412 nm) relative to K^+ (effective radii = 0.331 nm) results in slower transport through the dense PANI layer.[46] Second, the positively charged PANI layer leads to a large Donnan potential for divalent cations including the blocked Ca^{2+}, since electrostatic repulsion effects are stronger for divalent cations.[46] Finally, the much larger dehydration energy of Ca^{2+} (ΔG_{dehy} = 1505 kJ mol^{-1}) relative to K^+ (ΔG_{dehy} = 295 kJ mol^{-1}) makes the transport of desolvated Ca^{2+} through the membrane less energetically favorable than K^+.[46]

When designing our modified cement electrolyser, we used a similar configuration to our previous three-compartment cement electrolyser, which had a BPM to decompose $CaCO_3$ and release Ca^{2+} and pure streams of CO_2, O_2, and H_2. The CO_2 could be utilized directly (*e.g.*, with electrolysis) without further processing[1] and the H_2 could be used as fuel for a subsequent thermal kiln or be fed back to the anode for the hydrogen oxidation reaction (HOR) to reduce the electrolysis voltage.[28] The key difference in the design was the composite CEM used to separate Ca^{2+} and OH^- production and combining enriched electrolytes in a dedicated reactor to produce the target product, $Ca(OH)_2$. This new design enabled us to generate the solid products in a separate chemical reactor without compromising the performance of the electrolyser and allowed us to optimize the electrochemical and chemical systems independently.

The electrolyser demonstrated in this study was operated as a batch process. However, for large-scale production, such as cement manufacturing, continuous operation is far more desirable. We hypothesize that our electrolyser can now be run continuously as $Ca(OH)_2$ precipitation no longer limits its stability. Furthermore, we satisfied the two criteria required for continuous electrochemical production of a cement clinker precursor by maintaining a steady-state pH in the chemical compartment that is low enough to dissolve $CaCO_3$, while simultaneously ensuring a high enough pH in the cathode compartment to precipitate $Ca(OH)_2$. Our future work will explore continuous electrochemical cement clinker precursor production.

The supporting electrolyte in this study was 1 M KCl. The presence of potassium and chloride in cement clinker can negatively impact the final product. Elevated levels of alkalis (Na and K) can decrease the final strength of the cement,[48] and promote the alkali-silica reaction, which can cause expansive stresses in concrete.[49,50] Alkali concentrations in cement below 0.60 wt% are generally preferred, which is the limit for ordinary Portland cement (all types, I–V) when mixed with aggregates that are potentially reactive.[19,51] Chloride ions pose another risk by accelerating the corrosion of the steel reinforcements in concrete.[21,52] The resulting oxidation of the iron in the steel bar generates internal stresses in the concrete and weakens the bar itself,[53,54] and is the most common mode of failure for reinforced concrete structures.[52] Chloride content in cement is limited to between 0.06–1.00 wt%, depending on the end use.[55]

In this work, we demonstrated that the $Ca(OH)_2$ produced by our electrolyser has concentrations of potassium and chloride well below the limits set on ordinary Portland cement. We also demonstrated the formation of calcium silicates by thermal clinkering of electrochemical $Ca(OH)_2$ with SiO_2 (Fig. S12, ESI†). This demonstrates that the $Ca(OH)_2$ produced by our electrolyser is suitable for use as a clinker precursor free of harmful impurities, and is capable of forming dicalcium silicate at 1050 °C and tricalcium silicate at 1500 °C in a kiln.

The arrangement of an electrolyser and calcium reactor in tandem to produce $Ca(OH)_2$ avoided the issues associated with $Ca(OH)_2$ accumulation in the cement electrolyser. A similar and alternative approach could involve operating an independent electrolyser to generate acid and base by splitting water, then reacting $CaCO_3$ with the acid and base in sequence to form $Ca(OH)_2$ (Fig. S15, ESI†). However, a major shortcoming of this approach is the current efficiency of the electrolyser used to generate acid and base. Two-compartment electrolysers using CEMs or anion exchange membranes suffer from the significant crossover of H^+ or OH^-, respectively. Consequently, the majority (as much as 95%) of electrochemically generated H^+ and OH^- are neutralized rather than being consumed in $Ca(OH)_2$ production. We fed $CaCO_3$ to the three-compartment electrolyser to react with H^+ *in situ* to mitigate H^+ crossover and avoid this issue. Our previously reported experiments established that 100% of electrochemically generated H^+ (*i.e.*, 100% current efficiency) can be utilized in reactions with $CaCO_3$.[1] In this work, we showed how to maintain this efficient utilization of electrochemically generated H^+ while increasing the durability of the electrolyser with a calcium reactor where Ca^{2+} reacts with the electrochemically generated OH^-.

In our system, we demonstrated a path to substantially reduce the capital expenditure (CAPEX) required for industrial operation of this process. By utilizing an integrated electrolyser to generate H^+ and OH^- *in situ*, we eliminated the need for the procurement, regeneration, and storage of large volumes of acids and bases. This minimizes the infrastructure investments, consequently reducing the overall CAPEX, a critical metric in the evaluation of new industrial processes (Fig. S16 and S17, ESI†).[56]

Our integrated electrolyser not only reduces the operational complexities, but also the risks associated with chlorine handling in traditional saltwater electrolysis.[57] By bypassing these intricacies, we streamlined the production process and enhanced its economic feasibility. The avoidance of potential regulatory, safety, and environmental costs associated with chlorine further contributes to the financial viability of our

approach, emphasizing the value of our integrated electrolyser system from a CAPEX perspective.

We compared the energy and CO_2 emissions intensity of a plant employing the cement electrolyser against a conventional thermal cement plant. For the energy analysis, we considered two voltages for the cement electrolyser, current performance (5 V), and an optimistic future case (2.5 V). We found that the thermal cement plant consumes less energy, 3.8 GJ ton^{-1} of cement, than the cement electrolyser at its current performance (13.1 GJ ton^{-1} of cement) or in the future performance case (7.8 GJ ton^{-1} of cement, Fig. 5). However, the gas stream of pure CO_2 exiting the chemical compartment of the cement electrolyser enabled direct integration of either carbon capture or utilization processes.[1,58] When combined with an amine scrubber, the cement electrolyser reduced CO_2 emissions by 67–73%, from 785 kg_{CO_2} ton^{-1} of cement for the thermal process to 254 and 209 kg_{CO_2} ton^{-1} of cement for the cement electrolyser with current (5 V) and future (2.5 V) performance, respectively (Fig. 6). This finding is consistent with our previous estimates.[1]

Conclusion

In summary, electrochemical methods for cement clinker precursor production have the potential to significantly reduce CO_2 emissions from cement production. However, a major operational issue for cement electrolysers is the deposition of the $Ca(OH)_2$ product on the CEM. This process increases cell voltages, damages the CEM, and limits electrolyser durability. To address this issue, we introduced a calcium reactor to form $Ca(OH)_2$ outside the electrolyser. A Ca^{2+}-blocking composite membrane, which we developed by chemically modifying a commercial CEM, decoupled electrochemistry from the chemistry. This design enabled the cement electrolyser to operate over 50 hours at 100 mA cm^{-2} with no notable increases in cell voltage. The effectiveness of the composite membrane was validated using an *operando* imaging system. This work represents an advance towards decarbonizing one of the highest-emitting manufacturing industries and describes a durable method for producing cement clinker precursors.

Author contributions

C. P. B. supervised the project. Z. Z. conceived the study. Z. Z., T. J., S. R., and A. S. R. W. designed experiments. Z. Z., A. S. R. W., and C. T. E. P. performed the experiments and B. A. W. M. and A. S. R. W. performed the analysis and made figures. B. A. W. M., Z. Z. wrote the first draft and generated the figures. Y. W. designed the 100 cm^2 electrolyser and made figures. All authors contributed to the final manuscript writing.

Data availability

The data supporting the findings in this study are available either within the paper and its ESI.†

Conflicts of interest

Berlinguette, C. P.; Zhang, Z.; Mowbray, B. A. W. ''Methods and Apparatus for Converting Metal Carbonate Salts to Metal Hydroxides''. PCT International Application no. PCT/CA2023/050064, filed January 20, 2023. Priority date: January 20, 2022. The remaining authors declare no other competing interests.

Acknowledgements

The authors are grateful to the New Frontiers in Research Fund (NFRFT-2022-00197), the Canadian Natural Science and Engineering Research Council (RGPIN-2018-06748), Canadian Foundation for Innovation (229288), Canadian Institute for Advanced Research (BSE-BERL-162173), and Canada Research Chairs for financial support. B.A.W.M. acknowledges funding from the Natural Sciences and Engineering Research Council of Canada doctoral fellowships. This research was undertaken thanks in part to funding from the Canada First Research Excellence Fund, Quantum Materials and Future Technologies Program.

References

1 Z. Zhang, B. A. W. Mowbray, C. T. E. Parkyn, C. T. E. Waizenegger, A. S. R. Williams, E. W. Lees, S. Ren, Y. Kim, R. P. Jansonius and C. P. Berlinguette, *Energy Environ. Sci.*, 2022, **15**, 5129–5136.
2 L. D. Ellis, A. F. Badel, M. L. Chiang, R. J.-Y. Park and Y.-M. Chiang, *Proc. Natl. Acad. Sci. U. S. A.*, 2020, **117**, 12584–12591.
3 A. Perego, D. Kulkarni, H.-M. Chang, X. Wang, J. Wei, M. Li and I. V. Zenyuk, *Meet. Abstr.*, 2021, **MA2021-02**, 840.
4 Q. Xie, L. Wan, Z. Zhang and J. Luo, *iScience*, 2023, **26**, 106015.
5 D. M. Weekes, D. A. Salvatore, A. Reyes, A. Huang and C. P. Berlinguette, *Acc. Chem. Res.*, 2018, **51**, 910–918.
6 S. Ren, D. Joulié, D. Salvatore, K. Torbensen, M. Wang, M. Robert and C. P. Berlinguette, *Science*, 2019, **365**, 367–369.
7 E. W. Lees, B. A. W. Mowbray, F. G. L. Parlane and C. P. Berlinguette, *Nat. Rev. Mater.*, 2021, **7**, 55–64.
8 T. Li, E. W. Lees, M. Goldman, D. A. Salvatore, D. M. Weekes and C. P. Berlinguette, *Joule*, 2019, **3**, 1487–1497.
9 E. W. Lees, M. Goldman, A. G. Fink, D. J. Dvorak, D. A. Salvatore, Z. Zhang, N. W. X. Loo and C. P. Berlinguette, *ACS Energy Lett.*, 2020, 2165–2173.
10 T. Li, E. W. Lees, Z. Zhang and C. P. Berlinguette, *ACS Energy Lett.*, 2020, 2624–2630.
11 Z. Zhang, E. W. Lees, F. Habibzadeh, D. A. Salvatore, S. Ren, G. L. Simpson, D. G. Wheeler, A. Liu and C. P. Berlinguette, *Energy Environ. Sci.*, 2022, **15**, 705–713.
12 Z. Zhang, E. W. Lees, S. Ren, B. A. W. Mowbray, A. Huang and C. P. Berlinguette, *ACS Cent. Sci.*, 2022, **8**, 749–755.

13 Z. Zhang, L. Melo, R. P. Jansonius, F. Habibzadeh, E. R. Grant and C. P. Berlinguette, *ACS Energy Lett.*, 2020, **5**, 3101–3107.
14 Y. Kim, E. W. Lees and C. P. Berlinguette, *ACS Energy Lett.*, 2022, **7**, 2382–2387.
15 G. Zhang, G. Yang, Q. Shen, S. Li, Z. Li, J. Liao, Z. Jiang, H. Wang, H. Zhang and W. Ye, *J. Power Sources*, 2022, **542**, 231740.
16 J. Peng, M. Tian, N. M. Cantillo and T. Zawodzinski, *Electrochim. Acta*, 2018, **282**, 544–554.
17 K. Hongsirikarn, J. G. Goodwin, S. Greenway and S. Creager, *J. Power Sources*, 2010, **195**, 7213–7220.
18 H. Farrokhzad, M. R. Moghbeli, T. Van Gerven and B. Van der Bruggen, *React. Funct. Polym.*, 2015, **86**, 161–167.
19 ASTM, C150 Standard Specification for Portland Cement, ASTM International, Jul7 26 2022.
20 J. L. Dalton, K. H. Gardner and B. J. Magee, *Resour., Conserv. Recycl.*, 2004, **41**, 227–241.
21 H. F. W. Taylor, *Cement Chemistry*, 2nd edn, Thomas Telford Publishing, 1997.
22 M. Fourmentin, G. Ovarlez, P. Faure, U. Peter, D. Lesueur, D. Daviller and P. Coussot, *Rheol. Acta*, 2015, **54**, 647–656.
23 Environment and Climate Change Canada, Emission Factors and Reference Values, **https://www.canada.ca/en/environment-climate-change/services/climate-change/pricing-pollution-how-it-will-work/output-based-pricing-system/federal-greenhouse-gas-offset-system/emission-factors-reference-values.html**, (accessed 1 February 2024).
24 Canadian Industry Program for Energy Conservation, Canadian cement industry energy benchmarking, Natural Resources Canada, 2009.
25 A. Mokhtar and M. Nasooti, *Energy Strategy Rev.*, 2020, **28**, 100458.
26 Canada's cement and concrete industry action plan to net-zero, Cement Association of Canada, 2023.
27 M. E. Boesch and S. Hellweg, *Environ. Sci. Technol.*, 2010, **44**, 9143–9149.
28 B. A. W. Mowbray, Z. B. Zhang, C. T. E. Parkyn and C. P. Berlinguette, *ACS Energy Lett.*, 2023, **8**, 1772–1778.
29 F. B. Juangsa, A. S. Cezeliano, P. S. Darmanto and M. Aziz, *S. Afr. J. Chem. Eng.*, 2022, **42**, 23–31.
30 Y. Wang, C. H. Sohn and J.-Y. Kim, *Therm. Sci. Eng. Prog.*, 2024, **47**, 102330.
31 A. Ilyushechkin, L. Schoeman, L. Carter and S. S. Hla, *Hydrogen*, 2023, **4**, 599–619.
32 CEMEX successfully deploys hydrogen-based ground-breaking technology, **https://www.cemex.com/w/cemex-successfully-deploys-hydrogen-based-ground-breaking-technology**, (accessed 23 September 2024).
33 HeidelbergCement produces cement with climate-neutral fuel mix using hydrogen technology, **https://www.heidelbergmaterials.com/en/pr-01-10-2021**, (accessed 23 September 2024).
34 S. Betancur, Argos implements an innovative hydrogen injection process at its Honduran oven for a more sustainable operation – Cementos Argos: Empresa multinacional líder y sostenible, **https://argos.co/argos-implements-an-innovative-hydrogen-injection-process-at-its-honduran-oven-for-a-more-sustainable-operation/**, (accessed 23 September 2024).
35 J. N. Knudsen, O. M. Bade, I. Askestad, O. Gorset and T. Mejdell, *Energy Procedia*, 2014, **63**, 6464–6475.
36 Global Status of CCS 2023, Global CCS Institute, 2023.
37 Brevik CCS – World's first CO_2-capture facility in the cement industry, **https://www.brevikccs.com/en/brevik-ccs-worlds-first-co2-capture-facility-in-the-cement-industry**, (accessed 20 September 2024).
38 Facilities – Global CCS Institute, **https://co2re.co/FacilityData**, (accessed 20 September 2024).
39 World's largest capture pilot plant for cement commissioned in China, **https://www.globalccsinstitute.com/news-media/insights/worlds-largest-capture-pilot-plant-for-cement-commissioned-in-china/**, (accessed 20 September 2024).
40 *2023 Environmental, Social, and Governance Report*, Anhui Conch Cement Company Ltd., 2024.
41 I. J. Uyanga and R. O. Idem, *Ind. Eng. Chem. Res.*, 2007, **46**, 2558–2566.
42 V. Buvik, K. K. Høisæter, S. J. Vevelstad and H. K. Knuutila, *Int. J. Greenhouse Gas Control*, 2021, **106**, 103246.
43 F. Vega, A. Sanna, B. Navarrete, M. M. Maroto-Valer and V. J. Cortés, *Greenhouse Gases: Sci. Technol.*, 2014, **4**, 707–733.
44 T. Hills, D. Leeson, N. Florin and P. Fennell, *Environ. Sci. Technol.*, 2016, **50**, 368–377.
45 A. G. Olabi, T. Wilberforce, K. Elsaid, E. T. Sayed, H. M. Maghrabie and M. A. Abdelkareem, *J. Cleaner Prod.*, 2022, **362**, 132300.
46 C. Tang and M. L. Bruening, *J. Polym. Sci.*, 2020, **58**, 2831–2856.
47 M. Andreeva, *Université Paris-Est*, Kuban State agrarian university, 2017.
48 I. Jawed and J. Skalny, *Cem. Concr. Res.*, 1978, **8**, 37–51.
49 T. E. Stanton, *Trans. Am. Soc. Civ. Eng.*, 1942, **107**, 54–84.
50 S. Diamond, *Cem. Concr. Compos.*, 1996, **18**, 205–215.
51 S. Diamond, *Cem. Concr. Res.*, 1976, **6**, 549–560.
52 S. Robuschi, A. Tengattini, J. Dijkstra, I. Fernandez and K. Lundgren, *Cem. Concr. Res.*, 2021, **144**, 106439.
53 Y. Tian, G. Zhang, H. Ye, Q. Zeng, Z. Zhang, Z. Tian, X. Jin, N. Jin, Z. Chen and J. Wang, *Constr. Build. Mater.*, 2023, **369**, 130504.
54 I. Fernandez and C. G. Berrocal, *Int. J. Concr. Struct. Mater.*, 2019, **13**, 1–19.
55 American Concrete Institute, Building Code Requirements for Structural Concrete ACI 318-19(22), American Concrete Institute, Farmington Hills, MI, 2019.
56 Kuldeep, W. D. Badenhorst, P. Kauranen, H. Pajari, R. Ruismäki, P. Mannela and L. Murtomäki, *Membranes*, 2021, **11**, 718–731.
57 S. Lokesh and R. Srivastava, *Energy Fuels*, 2022, **36**, 13417–13450.
58 D. J. D. Pimlott, A. Jewlal, B. A. W. Mowbray and C. P. Berlinguette, *ACS Energy Lett.*, 2023, **8**, 1779–1784.

